JACS
JOURNAL OF THE AMERICAN CHEMICAL SOCIETY
Communication
pubs.acs.org/JACS

Mg−Zr Cosubstituted Ta_3N_5 Photoanode for Lower-Onset-Potential Solar-Driven Photoelectrochemical Water Splitting

Jeongsuk Seo,[†] Tsuyoshi Takata,[‡] Mamiko Nakabayashi,[§] Takashi Hisatomi,[†] Naoya Shibata,[§] Tsutomu Minegishi,[†] and Kazunari Domen*[,†]

[†]Department of Chemical System Engineering, School of Engineering, The University of Tokyo, 7-3-1 Hongo, Bunkyo-ku, Tokyo 113-8656, Japan

[‡]Global Research Center for Environment and Energy Based on Nano1materials Science (GREEN), National Institute for Materials Science (NIMS), 1-1 Namiki, Tsukuba-city, Ibaraki 305-0044, Japan

[§]Institute of Engineering Innovation, The University of Tokyo, 2-11-16 Yayoi, Bunkyo-ku, Tokyo 113-8656, Japan

Supporting Information

ABSTRACT: In p/n photoelectrochemical (PEC) cell systems, a low onset potential for the photoanode, as well as a high photocurrent, are critical for efficient water splitting. Here, we report a Mg−Zr cosubstituted Ta_3N_5 (Ta_3N_5:Mg+Zr) photoanode, designed to provide a more negative onset potential for PEC water splitting. The anodic photocurrent onset on Ta_3N_5:Mg+Zr was 0.55 V_{RHE} under AM 1.5G-simulated sunlight, which represented a negative shift from the ca. 0.8 V_{RHE} for pure Ta_3N_5. This negative shift in the onset potential of PEC water splitting was attributed to the change in the bandgap potential due to partial substitution by the foreign ions Mg^{2+} and/or Zr^{4+}.

Water splitting into hydrogen and oxygen by solar energy is an attractive way to produce clean and renewable energy. Photoelectrochemical (PEC) water splitting on semiconductor electrodes is expected to become a widespread means of efficient solar energy conversion. For PEC water splitting, several cell configurations have been proposed:[1] half-cells (p-type/n-type photoelectrode and a counter electrode) assisted by an external bias and p/n PEC cells electrically combining photocathodes with photoanodes. Among these, p/n PEC cells are considered to be a more efficient route for unassisted water splitting. Despite the remarkable recent progress in the development of p-type photocathodes,[2,3] many challenging tasks still remain in n-type photoanodes. Specifically, the onset potential of the photoanodic current in PEC water splitting is too positive, which hampers the realization of p/n PEC water splitting devices. Therefore, the development of efficient photoanodes with a more negative photocurrent onset is highly desirable.

Several nitrides and oxynitrides (e.g., Ta_3N_5, $LaTaON_2$, $LaTiO_2N$, $BaTaO_2N$, etc.) with optical absorption at 600 nm or longer have been identified as attractive semiconductor photocatalysts/photoanodes in terms of having suitable bandgaps for splitting water under visible light.[4−7] In particular, Ta_3N_5, which has an anosovite (Ti_3O_5) structure consisting of corner- and edge-sharing TaN_6 octahedra, is a promising candidate for efficient PEC water splitting. Owing to its simple composition, there are various routes to fabricating a photoanode using this material. Thus, the PEC activity of Ta_3N_5 photoanodes has been improved by incorporating different structures such as particulates, nanorods, and thin films, and by modifying the surface of the electrode with a cocatalyst.[4,8−10] The photoanodic current at 1.23 V_{RHE} increased significantly by those attempts, whereas the photocurrent onset remained more positive than 0.8 V_{RHE} in most cases. The high onset potential, indicative of poor photoactivity, suggests the limitation of pure Ta_3N_5 as a photoanode.

Compositional modification by introducing foreign ions is a typical strategy to adjust semiconductor properties, which has led to enhanced photoelectrolysis/catalysis in many successful cases. For example, doping of the Ta_3N_5 electrode with Na^+ or Ba^{2+} was reported to enhance PEC water splitting.[11,12] Since 6-coordinate Na^+ (102 pm) and Ba^{2+} (135 pm) have significantly larger ionic radii than 6-coordinate Ta^{5+} (64 pm), the isostructural replacement of Ta^{5+} with Na^+ or Ba^{2+} in the anosovite structure is crystallographically unfavorable and leads to phase separation under heavy doping.[11,13] Mg^{2+} (72 pm) and Zr^{4+} (72 pm), with ionic radii comparable to that of Ta^{5+}, are suitable foreign ions for forming Ta_3N_5 variants. Owing to the difference in valence between the foreign and parent cations, the substitution of Mg^{2+} or Zr^{4+} for Ta^{5+} concurrently causes N^{3-}/O^{2-} replacement to maintain the charge balance, creating an oxynitride, $Ta_{3-x}Mg_xN_{5-3x}O_{3x}$ or $Ta_{3-x}Zr_xN_{5-x}O_x$, respectively. Thus, isostructural substitution is feasible for these foreign ions over a wide compositional range.[14,15]

In the present work, we fabricated Mg- and/or Zr-substituted Ta_3N_5 electrodes by the particle transfer (PT) method[5] with the appropriate powder samples, exploiting the flexibility in the fabrication route. The prepared Ta_3N_5-variant photoanodes were evaluated for water splitting photoactivity through various PEC measurements. Here, we report that the cointroduction of foreign Mg^{2+} and Zr^{4+} into Ta_3N_5 at high substitution levels caused an obvious negative shift in the onset potential for PEC water oxidation. In addition, the effect of Mg and/or Zr substitution on PEC activity will be explained on the basis of band gap potentials. Photocatalysis of the Ta_3N_5 variants in

Received: August 7, 2015
Published: October 1, 2015

DOI: 10.1021/jacs.5b08329
J. Am. Chem. Soc. 2015, 137, 12780−12783

powder form will also be discussed to support their enhanced PEC activities relative to that of pure Ta_3N_5.

The powder Ta_3N_5 variants were synthesized by flux-assisted nitridation using the corresponding oxide precursors along with a Na_2CO_3 flux under NH_3 flow at 1173 K. The oxide precursors were prepared by heating Ta_2O_5 mixed with $ZrO(NO_3)_2{\cdot}2H_2O$ and/or $Mg(NO_3)_2{\cdot}6H_2O$ at 923 K in air. The ratio of Mg:Zr in the cosubstituted photocatalysts is 1:2 unless otherwise noted. The synthesized Ta_3N_5 photocatalysts replaced with no ions, Mg^{2+}, Zr^{4+}, and Mg^{2+} + Zr^{4+} will be denoted as Ta_3N_5, Ta_3N_5:Mg, Ta_3N_5:Zr, and Ta_3N_5:Mg+Zr, respectively. For comparison, a typical Ta_3N_5 sample (hereafter "Ta_3N_5 (no flux)") was also nitrided from Ta_2O_5 in the absence of a Na_2CO_3 flux.[16] The photoelectrodes, which were fabricated by the PT method, consisted of an absorber particle layer, Nb ohmic contact layer, and Ti current collector layer. Subsequently, a bilayered Co−Fe oxide (hereafter "CoO_x-FeO_x") as cocatalyst was deposited on the photoanodes by pulse-current electrodeposition. PEC water splitting was performed in a conventional three-electrode system under simulated sunlight irradiation (AM1.5G). Further details of the experimental procedures are given in the Supporting Information (SI).

The crystal structures of the synthesized Ta_3N_5, Ta_3N_5:Mg, Ta_3N_5:Zr, and Ta_3N_5:Mg+Zr were determined by XRD in Figure 1. The replacement of Ta^{5+} with Mg^{2+} and/or Zr^{4+} was fixed to 33

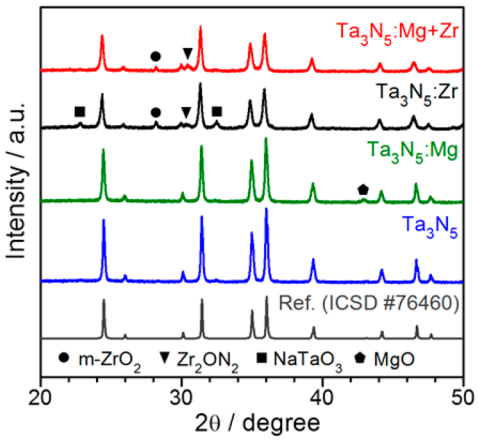

Figure 1. XRD patterns for Ta_3N_5, Ta_3N_5:Mg, Ta_3N_5:Zr, and Ta_3N_5:Mg +Zr photocatalysts synthesized by nitriding at 1173 K for 20 h under NH_3 flow.

at %, which was optimized by PEC water splitting activity. All photocatalysts showed XRD patterns assignable to the anosovite (Ti_3O_5) structure, but the Ta_3N_5 variants that underwent elemental substitution also exhibited small amounts of segregated phases such as ZrO_2, Zr_2ON_2, $NaTaO_3$, and MgO. The (110) peaks of Mg^{2+} and/or Zr^{4+}-substituted Ta_3N_5 slightly shifted toward lower angles as compared to that of Ta_3N_5, indicating the small lattice expansion by increased average ionic radii (Figure S1 in SI). ICP and O/N analysis revealed that the cosubstitution of Mg and Zr was accompanied by the O/N substitution to compensate an imbalance of ionic charge (Table S1 in SI). Although Mg^{2+} and Zr^{4+} have 12% larger ionic radii than Ta^{5+}, the concurrent substitution of smaller O^{2-} for N^{3-} reduced the extent of lattice expansion.

Figure 2 and Figure S2 in SI show the photocurrent−potential (I−E) curves for various Ta_3N_5 variant electrodes modified with and without CoO_x-FeO_x, respectively, under chopped AM1.5G

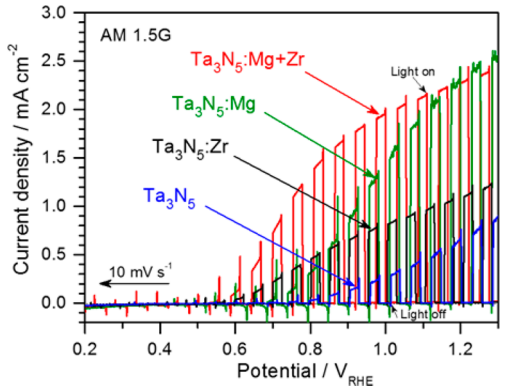

Figure 2. LSVs for CoO_x-FeO_x/Ta_3N_5, Ta_3N_5:Mg, Ta_3N_5:Zr, and Ta_3N_5:Mg+Zr photoanodes toward PEC water splitting under chopped AM1.5G sunlight. The measurements were performed by cathodically sweeping the potential from 1.3 to 0.2 V_{RHE} at a scan rate of 10 mV s^{-1} in a stirred Ar-saturated 0.1 M aqueous Na_2SO_4 electrolyte adjusted to pH 13.

sunlight. The anodic photocurrent was generated on the Ta_3N_5 electrode at around 0.82 V_{RHE} and gently increased above this potential, reaching 0.72 mA cm^{-2} at 1.23 V_{RHE}. Ta_3N_5 (no flux) exhibited an almost identical photocurrent onset at 0.78 V_{RHE} but a higher photocurrent (Figure S3 in SI). The lower photocurrent for the Ta_3N_5 would be attributable not only to the contamination of flux after the nitridation but also to different morphology of the synthesized photocatalysts (Figure S4 in SI). Thus, irrespective of the photocurrent, the onset potential was determined to be ca. 0.80 V_{RHE}, which likely reflected the inherent PEC activity of Ta_3N_5 prepared by the PT method. On the Ta_3N_5:Zr electrode, the onset potential was observed at 0.57 V_{RHE}, which clearly represented a shift toward more negative potential relative to that for the Ta_3N_5 electrode. The Ta_3N_5:Mg electrode generated an anodic photocurrent above 0.70 V_{RHE}, which represents a relatively small negative shift in onset potential. However, at 1.23 V_{RHE}, it generated a photocurrent twice as high as that for Ta_3N_5:Zr. The Ta_3N_5:Mg+Zr photoanode exhibited a lower onset potential at 0.55 V_{RHE} and a photocurrent of 2.3 mA cm^{-2} at 1.23 V_{RHE}. Note that the onset for Ta_3N_5:Mg+Zr was almost identical to that for the Ta_3N_5:Zr electrode, and its photocurrent increased more steeply than those for Ta_3N_5:Mg and Ta_3N_5:Zr. The cosubstituted Ta_3N_5 nitrided with no flux was prepared for comparison. The lower PEC activity revealed that the flux-assisted nitridation was very effective to synthesize the heavily substituted Ta_3N_5 with higher crystallinity (Figure S5 in SI). Moreover, a different Mg:Zr ratio (= 2:1) was examined, and it was found that the PEC activity was almost unchanged (Figure S6 in SI). The significantly different PEC activity induced by Mg and Zr cosubstitution points to a synergetic effect of the two single substitutions: Zr causes a negative shift in the onset potential, while Mg increases the photocurrent.

The cosubstitution of Mg^{2+} and Zr^{4+} enhanced the PEC activity over the compositional range of 14−43 at %, demonstrating the effectiveness of heavy substitution (Figure S7 in SI). Moreover, Ta_3N_5:Mg+Zr with 33 at % substitution showed the highest PEC activity among the various compositions examined. Clearly, the observed enhancements were not attributable to the byproduct phases originating from Mg and Zr additives (Figure S8 in SI). The UV−vis DRS spectra for the Ta_3N_5 variants showed that the optical absorption edge of each

DOI: 10.1021/jacs.5b08329
J. Am. Chem. Soc. 2015, 137, 12780−12783

powder was almost unchanged regardless of the type of substitution (Figure S9 in SI). This is most likely because the constituent orbitals for the conduction and valence band edges are invariably Ta 5d and N 2p states, respectively.[17] This also ruled out the possibility that the enhanced PEC activities were caused solely by the changed bandgap energies. Microgas chromatography demonstrated that H_2 and O_2 gases evolved during PEC water splitting in the stoichiometric ratio of 2:1 and almost achieved a Faradaic efficiency of unity (Figure S10 in SI). This indicates that the anodic photocurrent indeed originated from the oxygen evolution reaction by water splitting.

Figure 3a plots the wavelength dependence of the incident photon-to-current conversion efficiency (IPCE) on the

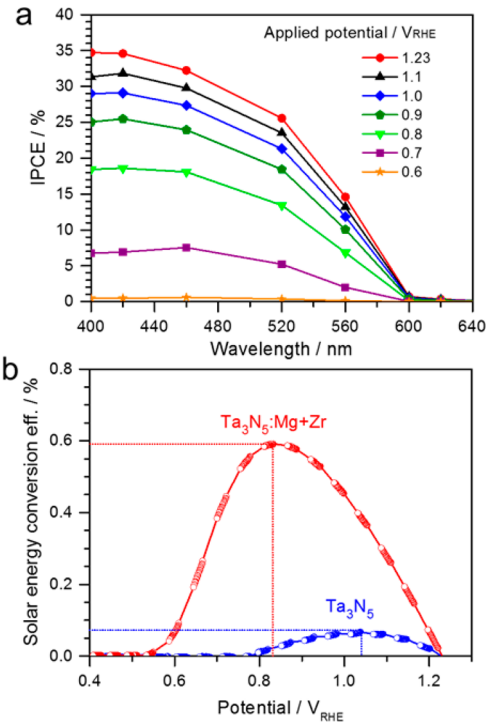

Figure 3. (a) Wavelength dependence of IPCE for the CoO_x-FeO_x/Ta_3N_5:Mg+Zr photoanode measured at different applied potentials between 0.6 and 1.23 V_{RHE}. (b) HC-STH conversion efficiencies (%) for the CoO_x-FeO_x/Ta_3N_5:Mg+Zr and CoO_x-FeO_x/Ta_3N_5 photoanodes.

Ta_3N_5:Mg+Zr photoanode measured at different applied potentials. The onset wavelengths for the photocurrents agreed well with the light absorption edge of Ta_3N_5:Mg+Zr. The IPCEs in the whole wavelength area increased significantly as the applied potential was increased from 0.6 to 0.8 V_{RHE}, and increased moderately above this potential. The IPCEs at 0.8 V_{RHE} were ca. 9−18% at 560−400 nm. In Figure 3b, half-cell solar-to-hydrogen (HC-STH) conversion efficiencies for the Ta_3N_5 and Ta_3N_5:Mg+Zr photoanodes are plotted as a function of applied potential, using the voltammograms shown in Figure 2. The HC-STH for Ta_3N_5 (no flux) was also presented (Figure S11 in SI). The maximum HC-STH conversion efficiency for Ta_3N_5:Mg+Zr was 0.59% at 0.82 V_{RHE}, indicating that the Ta_3N_5:Mg+Zr photoanode operated most effectively in the case of PEC water splitting around 0.8 V_{RHE}. Upon substitution with Mg^{2+} and Zr^{4+}, the potential at which HC-STH was maximized shifted by 0.2 V_{RHE} in the negative direction. This is favorable for unassisted water splitting using p/n PEC cells.

The microstructure of Ta_3N_5:Mg+Zr was characterized by SEM analysis (Figure S4 in SI). Broadly speaking, two types of particle morphologies were observed: particles a few hundred nanometers in size and larger columnar particles. The columnar crystallites were observed only in the case of Ta_3N_5:Mg+Zr, while the other samples consisted mostly of particles a few hundred nanometers in size. Moreover, HRTEM and SAED revealed clear lattice fringes and the corresponding Ta_3N_5 diffraction pattern for a columnar particle, indicating the single crystallinity of the anosovite structure (Figure S12 in SI). Figure 4 shows a typical cross-sectional TEM image and the

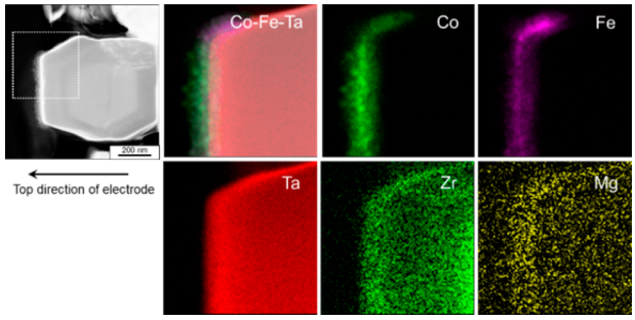

Figure 4. Cross-sectional STEM image and elemental EDS mapping results for a single Ta_3N_5:Mg+Zr particle loaded on a photoanode fabricated by the PT method. EDS mapping was conducted inside the white square in the STEM image. The elements Co and Fe derive from the cocatalyst CoO_x-FeO_x electrodeposited on the photoanode. Ta, Zr, and Mg represent the constituent elements of the Ta_3N_5:Mg+Zr.

corresponding EDS mapping for the CoO_x-FeO_x/Ta_3N_5:Mg+Zr electrode. The EDS elemental mapping demonstrated that Mg and Zr were homogeneously distributed inside a single particle, indicating that the foreign ions were incorporated into the Ta_3N_5 crystal structure. It was also found that the bilayered CoO_x/FeO_x was deposited only on top of the particle, i.e., on the exposed surface of the photoelectrode. No large columnar particles were observed in the Ta_3N_5:Mg+Zr nitride sample using three times the normal amount of Na_2CO_3 flux, but the onset potential was identical (Figure S13 in SI). This suggests that the negative shift in the onset potential for PEC water splitting was mainly due to changes in the semiconducting properties of Ta_3N_5 induced by the substitution, rather than to morphological changes.

The band positions and flat band potentials (E_{fb}) of Ta_3N_5 and Ta_3N_5:Mg+Zr were investigated by Tauc plots, PESA spectra, and MS plots to discuss their semiconductor properties (Figure S14 in SI). A detailed discussion is presented in the Supporting Information. Figure 5 shows the expected band diagrams for Ta_3N_5 and Ta_3N_5:Mg+Zr. The conduction and valence band edges for Ta_3N_5 were estimated to be −0.6 and 1.5 V_{NHE} (pH = 0). However, Ta_3N_5:Mg+Zr had conduction and valence band edges at −0.8 and 1.35 V_{NHE} (pH = 0), respectively. The E_{fb} values for Ta_3N_5 and Ta_3N_5:Mg+Zr, which were determined to be −0.18 and −0.43 V_{NHE}, respectively, shifted nearly in parallel to more negative onset potentials upon Mg−Zr cosubstitution. The negative shift in band gap potential is presumably due to the incorporation of more cationic ions (Mg^{2+} and Zr^{4+}) than Ta^{5+}. It is thought that the observed negative shift in the energy levels contributed to the lower onset potential for the Ta_3N_5:Mg+Zr photoanode.

In addition, the photocatalytic activity of Ta_3N_5 variants in powder suspension form was measured by conducting H_2 and O_2

DOI: 10.1021/jacs.5b08329
J. Am. Chem. Soc. 2015, 137, 12780−12783

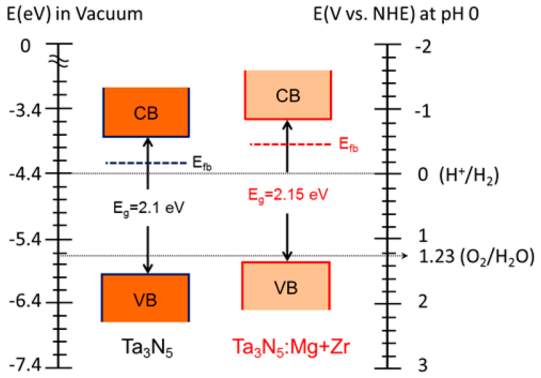

Figure 5. Band structure diagram of Ta_3N_5 and Ta_3N_5:Mg+Zr.

evolution separately in the presence of MeOH and Ag^+ as a sacrificial electron donor and acceptor, respectively. As seen in Figures S15 and S16 and Table S2 in SI, the photocatalytic activity changed markedly with the type of substitution. Mg and Zr single substitutions enhanced the H_2 evolution several times, but reduced the O_2 evolution capacity noticeably. The activity of Ta_3N_5:Mg+Zr (25 at%) for H_2 evolution was approximately 15 times higher than that of Ta_3N_5, while the O_2 evolution for the former was lower. These results corroborated the synergetic effect of the incorporated Mg and Zr, as discussed in the PEC examination above. Some of the elementary steps of photocatalysis are not identical to those of photoelectrolysis. However, the results of photocatalysis also indicate changes in semiconductor properties by compositional modification. The changes in H_2 and O_2 evolution capacity could be due to the observed shift in band position.

In summary, compositional modification of Ta_3N_5 by partial substitution with foreign ions was demonstrated to be effective in enhancing PEC water splitting activity. Mg−Zr cosubstitution influenced the onset potential and photocurrent by a sort of synergetic effect so that a relatively large photocurrent at a more negative potential was obtained, recording a 0.59% HC-STH conversion efficiency at 0.82 V_{RHE}. Although a dramatic improvement in photocurrent onset was achieved by compositional modification, the HC-STH value was still lower than the state-of-the-art Ba-doped Ta_3N_5 nanorod photoanode (ca. 1.4% at the same potential).[13] The present flux-assisted nitridation method might be suitable for synthesizing a multicomponent oxynitride. Improving the synthesis method for multicomponent (oxy)nitride materials is key to further enhancing the photocurrent in addition to lowering the onset potential. The strategy of compositional modification demonstrated in the present study is expected to be applicable to a wide range of semiconductors and would enable the fabrication of more efficient photoelectrodes.

■ ASSOCIATED CONTENT

Supporting Information

The Supporting Information is available free of charge on the ACS Publications website at DOI: 10.1021/jacs.5b08329.

Preparations of photocatalysts and photoanodes; physical characterization of photocatalysts; supplemental PEC activity; discussion of band structure (PDF)

■ AUTHOR INFORMATION

Corresponding Author

*domen@chemsys.t.u-tokyo.ac.jp

Notes

The authors declare no competing financial interest.

■ ACKNOWLEDGMENTS

This work was supported by a Grant-in-Aid for Specially Promoted Research (No. 23000009) and A3 Foresight Program of the Japan Society for the Promotion of Science (JSPS) and by Nanotechnology Platform (No. 12024046) and Development of Environmental Technology using Nanotechnology of the Ministry of Education, Culture, Sports, Science and Technology (MEXT), Japan. We thank the Material Analysis Station at NIMS for ICP measurement and O/N analysis.

■ REFERENCES

(1) Seitz, L. C.; Chen, Z.; Forman, A. J.; Pinaud, B. A.; Benck, J. D.; Jaramillo, T. F. *ChemSusChem* **2014**, *7*, 1372.
(2) Paracchino, A.; Laporte, V.; Sivula, K.; Gratzel, M.; Thimsen, E. *Nat. Mater.* **2011**, *10*, 456.
(3) Kumagai, H.; Minegishi, T.; Sato, N.; Yamada, T.; Kubota, J.; Domen, K. J. *J. Mater. Chem. A* **2015**, *3*, 8300.
(4) Li, Y.; Takata, T.; Cha, D.; Takanabe, K.; Minegishi, T.; Kubota, J.; Domen, K. *Adv. Mater.* **2013**, *25*, 125.
(5) Minegishi, T.; Nishimura, N.; Kubota, J.; Domen, K. *Chem. Sci.* **2013**, *4*, 1120.
(6) Feng, J.; Luo, W.; Fang, T.; Lv, H.; Wang, Z.; Gao, J.; Liu, W.; Yu, T.; Li, Z.; Zou, Z. *Adv. Funct. Mater.* **2014**, *24*, 3535.
(7) Ueda, K.; Minegishi, T.; Clune, J.; Nakabayashi, M.; Hisatomi, T.; Nishiyama, H.; Katayama, M.; Shibata, N.; Kubota, J.; Yamada, T.; Domen, K. *J. Am. Chem. Soc.* **2015**, *137*, 2227.
(8) Higashi, M.; Domen, K.; Abe, R. *Energy Environ. Sci.* **2011**, *4*, 4138.
(9) Liao, M.; Feng, J.; Luo, W.; Wang, Z.; Zhang, J.; Li, Z.; Yu, T.; Zou, Z. *Adv. Funct. Mater.* **2012**, *22*, 3066.
(10) Li, M.; Luo, W.; Cao, D.; Zhao, X.; Li, Z.; Yu, T.; Zou, Z. *Angew. Chem., Int. Ed.* **2013**, *52*, 11016.
(11) Kado, Y.; Hahn, R.; Lee, C.-Y.; Schmuki, P. *Electrochem. Commun.* **2012**, *17*, 67.
(12) Li, Y.; Zhang, L.; Torres-Pardo, A.; Gonzalez-Calbet, J. M.; Ma, Y.; Oleynikov, P.; Terasaki, O.; Asahina, S.; Shima, M.; Cha, D.; Zhao, L.; Takanabe, K.; Kubota, J.; Domen, K. *Nat. Commun.* **2013**, *4*, 2566.
(13) Kado, Y.; Lee, C. Y.; Lee, K.; Muller, J.; Moll, M.; Spiecker, E.; Schmuki, P. *Chem. Commun.* **2012**, *48*, 8685.
(14) Guenther, E.; Jansen, M. *Mater. Res. Bull.* **2001**, *36*, 1399.
(15) Schilling, H.; Lerch, M.; Börger, A.; Wolff, K. D.; Dronskowski, R.; Bredow, T.; Tovar, M.; Baehatz, C. *J. Solid State Chem.* **2006**, *179*, 2416.
(16) Takata, T.; Lu, D. L.; Domen, K. *Cryst. Growth Des.* **2011**, *11*, 33.
(17) Chun, W.-J.; Ishikawa, A.; Fujisawa, H.; Takata, T.; Kondo, J. N.; Hara, M.; Kawai, M.; Matsumoto, Y.; Domen, K. *J. Phys. Chem. B* **2003**, *107*, 1798.

DOI: 10.1021/jacs.5b08329
J. Am. Chem. Soc. 2015, 137, 12780−12783